

Membrane Curvature Induced by Aggregates of LH2s and Monomeric LH1s

Danielle E. Chandler, James Gumbart, John D. Stack, Christophe Chipot, and Klaus Schulten*

Department of Physics and Beckman Institute, University of Illinois at Urbana-Champaign, Urbana, Illinois

ABSTRACT The photosynthetic apparatus of purple bacteria is contained within organelles called chromatophores, which form as extensions of the cytoplasmic membrane. The shape of these chromatophores can be spherical (as in *Rhodobacter sphaeroides*), lamellar (as in *Rhodospseudomonas acidophila* and *Phaeospirillum molischianum*), or tubular (as in certain *Rb. sphaeroides* mutants). Chromatophore shape is thought to be influenced by the integral membrane proteins Light Harvesting Complexes I and II (LH1 and LH2), which pack tightly together in the chromatophore. It has been suggested that the shape of LH2, together with its close packing in the membrane, induces membrane curvature. The mechanism of LH2-induced curvature is explored via molecular dynamics simulations of multiple LH2 complexes in a membrane patch. LH2s from three species—*Rb. sphaeroides*, *Rps. acidophila*, and *Phsp. molischianum*—were simulated in different packing arrangements. In each case, the LH2s pack together and tilt with respect to neighboring LH2s in a way that produces an overall curvature. This curvature appears to be driven by a combination of LH2's shape and electrostatic forces that are modulated by the presence of well-conserved cytoplasmic charged residues, the removal of which inhibits LH2 curvature. The interaction of LH2s and an LH1 monomer is also explored, and it suggests that curvature is diminished by the presence of LH1 monomers. The implications of our results for chromatophore shape are discussed.

INTRODUCTION

Chromatophores are extensions of the bacterial cytoplasmic membrane that form to house the photosynthetic apparatus in purple photosynthetic bacteria. There is a wealth of information on chromatophore structures, not least because the bacterial photosynthetic unit has long been studied as an exemplary photosynthetic system (see (1–3) for reviews). There is significant variation in chromatophore shape among species, including small vesicles in *Rhodobacter sphaeroides* and *Rhodobacter capsulatus*, flat lamellar folds in *Rhodospseudomonas acidophila* and *Phaeospirillum molischianum*, and long tubules in certain *Rb. sphaeroides* mutants (4–6). It is known that these structures (vesicles, folds, or tubes) form directly after the aggregation of the Light-Harvesting Complexes I and II (LH1 and LH2) in the cytoplasmic membrane, so it is tempting to think that the aggregation of these proteins induces chromatophore formation. Recent molecular dynamics and Monte Carlo simulations have explored the connection between aggregation and structure formation, finding that the individual LH1 and LH2 proteins can induce curvature (7), and that the aggregation of many curvature-inducing bodies can cause chromatophore vesiculation (8).

This report extends the preliminary work done in Chandler et al. (7), where it was found that hexagonally packed aggregates of seven LH2s could interact in a way that produces an

overall curvature. Here, we further explore the factors underlying this curvature behavior and suggest that it arises from a combination of packing and electrostatic interactions. We also find that aggregates of LH2s from all species induce curvature, regardless of the natural chromatophore shape of those species (see Fig. 1 for a full sequence comparison). In particular, it came as some surprise that LH2s from *Rps. acidophila* and *Phsp. molischianum* induce curvature, since both of these species have lamellar chromatophores. We previously suggested that since both of these species contain monomeric LH1s, perhaps the interaction of LH1 monomers with LH2s reduces the overall curvature. We explored these LH1-LH2 interactions by simulating an LH1 monomer surrounded by LH2s, finding that the curvature induced in this case is indeed substantially less than that induced by LH2s alone. The results reported here represent simulations of 880,000–1.7 million atoms, over a combined total time of 170 ns.

METHODS

LH2 assemblies

Several LH2 assemblies were constructed; all contain seven LH2s placed in a 300×300 Å nonperiodic membrane patch composed of 50% 1-palmitoyl-2-oleoylphosphatidylethanolamine (POPE) and 50% 1-palmitoyl-2-oleoylphosphatidylglycerol (POPG) lipids; an example system is depicted in Fig. 2 E. As discussed in Chandler et al. (7), the system was constructed so that water separates the membrane patch from its periodic images, due to the concern that a continuous membrane would resist curvature. There are several experimental reports on the lipid content of purple bacterial cytoplasmic and chromatophore membranes, which suggest that the membrane mainly consists of phosphatidylethanolamine (PE), phosphatidylglycerol (PG), and phosphatidylcholine (PC) lipids, but which are inconsistent in terms of individual percentages (9–12). Additionally, the distribution of the

Submitted December 29, 2008, and accepted for publication September 3, 2009.

*Correspondence: kschulte@ks.uiuc.edu

Christophe Chipot is on leave from Équipe de Dynamique des Assemblages Membranaires, UMR CNRS/UHP 7565, Nancy Université BP 239, Nancy, France.

Editor: Reinhard Lipowsky.

© 2009 by the Biophysical Society
0006-3495/09/12/2978/7 \$2.00

doi: 10.1016/j.bpj.2009.09.007

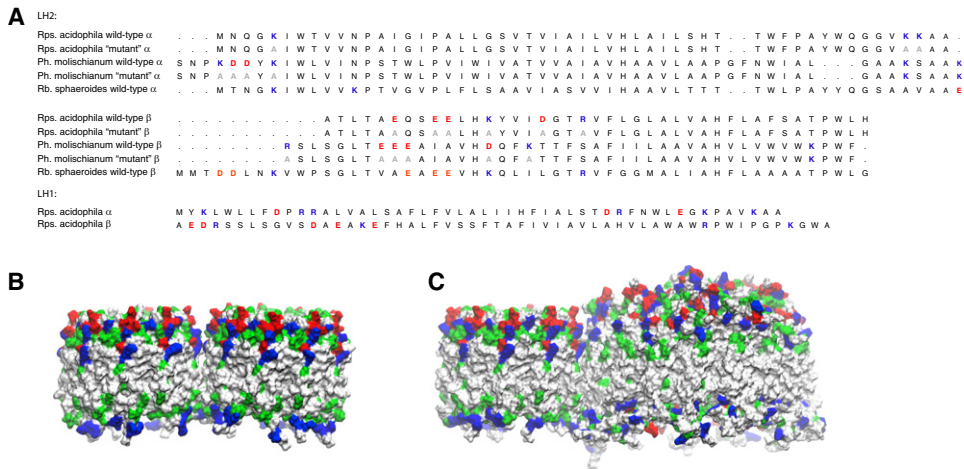


FIGURE 1 (A) Sequences of the wild-type and altered α - and β -proteins for *Rps. acidophila*, *Phsp. molischianum*, and *Rb. sphaeroides* used in the simulations. Positively charged residues are highlighted in blue, negatively charged residues in red, and replacement alanines in gray. Green and white represent polar and nonpolar residues, respectively. (B) Two adjacent *Rps. acidophila* LH2s, showing the location of charged residues. (C) The LH1 monomer with adjacent LH2, again showing the location of the charged residues. The majority of the charged residues on the LH1 β -chain are located on a flexible region above where the LH2 contacts the LH1. The cytoplasmic side is the top side of the protein in our representations.

charged PG lipids is likely to be asymmetric, with the majority of the PG found on the periplasmic side of the membrane (13). We chose a simple, symmetric lipid distribution to decouple the curvature effect due to the LH2 proteins from any possible spurious peripheral effect resulting from an asymmetric lipid distribution.

Two packing arrangements were considered, referred to as the closely packed and sparsely packed arrangements. In the closely packed arrangement, adjacent LH2s are in direct contact, with no lipids in between; in the sparsely packed arrangement, approximately a single layer of lipids separates adjacent LH2s. The mutual rotational orientation of the LH2s is not known, as atomic force microscopy (AFM) images do not show this level of detail. In our simulations, we chose to translate each of the outer ring LH2s away from the central one without rotating it. However, due to the ninefold symmetry of *Rps. acidophila* LH2 (eightfold for *Phsp. molischianum*) the rotational orientation can matter only within a range of 40–45°. We simulated LH2s from three species, using the crystal structures for *Rps. acidophila* and *Phsp. molischianum*, and a homology model for *Rb. sphaeroides*, as described in Chandler et al. (7). To probe the importance of charged residues on LH2 curvature, we created both mutant *Rps. acidophila* and *Phsp. molischianum* LH2s by mutating charged residues to alanine, as well as neutral LH2s by replacing the charged residues with their uncharged analogs (14). In each case, the membrane patch was placed in a water box composed of explicit TIP3 water, and the system charge was neutralized by the addition of sodium ions. The set of simulations performed

is listed in Table 1 (simulations from Chandler et al. (7) are included to compare with new data).

All systems were first energy-minimized and equilibrated in the NVT ensemble for 0.5 ns with all atoms except the lipid acyl chains harmonically restrained. The system was then equilibrated in the NPT ensemble with only the protein and pigments restrained for ~150 ps to allow water molecules to hydrate the membrane-protein assembly and the size of the simulation cell to stabilize. Finally, the system was equilibrated in the NPT ensemble without restraints. Simulations were performed using NAMD 2.6 (15) and the CHARMM27 force field with CMAP corrections (16,17). The equations of motion were integrated using a multiple time-stepping algorithm in which bonded interactions were evaluated every 1 fs, short-range nonbonded interactions every 2 fs, and long-range electrostatics interactions every 4 fs. Short-range nonbonded interactions were truncated smoothly with a spherical cutoff radius of 12 Å, and a switching distance of 10 Å. Long-range electrostatic interactions were calculated with the particle-mesh Ewald method (18), with a grid point density of $\sim 1/\text{Å}^3$.

LH1 monomer

Modeling of a *Rps. acidophila* LH1 monomer began from the *Rb. sphaeroides* LH1-RC-PufX model (note that PufX is a small protein consisting of a single transmembrane helix, the presence of which induces LH1 to form dimers rather than monomers) constructed in Chandler et al. (7).

TABLE 1 Summary of simulations performed

System	Time	Atoms	Water	Ions	POPE	POPG	Box (Å)
Seven <i>Rps. acidophila</i> LH2s (closely packed)	20 ns	996,535	216,475	868	874	868	350 × 350 × 87
Seven <i>Rps. acidophila</i> LH2s (sparsely packed)	14 ns	988,391	216,607	813	862	813	350 × 350 × 87
Seven <i>Rb. sphaeroides</i> LH2s (closely packed)	17.5 ns	959,379	204,402	954	849	828	330 × 330 × 95
Seven <i>Rb. sphaeroides</i> LH2s (sparsely packed)	14 ns	970,485	206,725	958	878	832	330 × 330 × 95
Seven <i>Phsp. molischianum</i> LH2s (closely packed)	18 ns	890,948	179,058	885	950	941	330 × 330 × 87
Seven <i>Rps. acidophila</i> LH2s charged residues → alanine (closely packed)	12 ns	880,857	179,005	938	880	875	330 × 330 × 87
Seven <i>Rps. acidophila</i> LH2s cyto. charged residues → alanine (closely packed)	11 ns	882,951	178,736	817	887	880	330 × 330 × 87
Seven <i>Rps. acidophila</i> LH2s charged residues neutralized (closely packed)	19 ns	1,075,455	242,782	930	874	868	330 × 330 × 105
Seven <i>Phsp. molischianum</i> LH2s charged residues → alanine (closely packed)	12 ns	887,690	179,804	762	950	930	330 × 330 × 87
Seven <i>Phsp. molischianum</i> LH2s charged residues neutralized (closely packed)	20 ns	1,082,926	243,051	940	950	941	330 × 330 × 105
One <i>Rps. acidophila</i> LH1 with seven LH2s (closely packed)	14 ns	1,677,754	400,958	1504	1192	1187	380 × 380 × 125

Because of the lack of a high-resolution structure for any of the components of the *Rps. acidophila* LH1-RC complex, homology models were built. LH1 α and LH1 β show 53% and 41% sequence identity, respectively, between *Rps. acidophila* and *Rb. sphaeroides*. As no sequences could be found for the *Rps. acidophila* reaction center (RC) components, the RC from *Rb. sphaeroides* was used (PDB entry 1PCR). Because the RC is enclosed by LH1, we do not believe it plays a significant role in LH1-LH2 interactions. A circular, symmetric ring of 16 LH1 α/β subunit pairs was built around the RC in accordance with the position of the RC in the *Rb. sphaeroides* LH1-RC monomer originally constructed in Hu and Schulten (19). The resulting model was placed in a mixed POPE/POPG bilayer, solvated above and below, and then simulated for 10 ns. The LH1 monomer adopted a slightly elliptical shape, with the major axis corresponding to that of the RC, as expected from experimental images (20–26). The 10-ns-equilibrated model of the LH1 monomer was then used for building the LH1/LH2 assembly. The LH1-LH2 system contained 1.7 million atoms and was simulated for 14 ns.

RESULTS

The curvature of the LH2 protein patch was analyzed by calculating the average tilt angle of the six peripheral LH2s with respect to the central one. Using the relation

$$R + \frac{h}{2} = \frac{d}{2\sin(\theta/2)}, \quad (1)$$

where h is the height of LH2 ($h = 50$ Å), d is the distance between the centers of two adjacent LH2s, θ is the tilt angle, and R is the radius of curvature, we can then convert the tilt angle to an approximate radius of curvature (see Fig. 2 F for derivation). For perspective, radii of vesicular chromatophores typically range from 150 to 400 Å (4). We analyze the curvature of the protein patch rather than the curvature of the surrounding lipids because the curvature arises from the packing of the proteins, with the lipids accommodating the curved hydrophobic transmembrane region of the proteins.

Sparse versus packed LH2 arrangements for *Rps. acidophila* and *Rb. sphaeroides*

We explored the effect of packing on LH2 curvature for two species, *Rps. acidophila* and *Rb. sphaeroides*. Tilt angle versus simulation time is plotted for each species and each packing arrangement in Fig. 2 A. The LH2 spacing for the sparse and packed systems were $d = 85$ Å and 77 Å, respectively. The *Rps. acidophila* and *Rb. sphaeroides* systems equilibrated to a final average tilt angle of $6.0^\circ \pm 0.4^\circ$ and $5.4^\circ \pm 0.3^\circ$, respectively, for the sparse arrangement. In the packed configuration, *Rps. acidophila* equilibrated to a final tilt angle of $8.6^\circ \pm 0.4^\circ$ and *Rb. sphaeroides* equilibrated to an angle of $12.9^\circ \pm 0.5^\circ$. The closer packing induced curvature more quickly and resulted in a substantially higher final tilt angle in each case, showing that LH2 curvature is sensitive to the degree of protein-protein packing. A tilt angle of 6° corresponds to a radius of curvature of ~ 790 Å, whereas 8° corresponds to 530 Å ($d = 77$ Å for this packing), and 13° corresponds to 315 Å.

Simulation of *Phsp. molischianum* LH2 and comparison of the three LH2 species

In addition to the previous simulations, a simulation was performed with closely packed *Phsp. molischianum* LH2s. *Phsp. molischianum* LH2 has only eight subunits, in contrast to the nine-subunit LH2s of *Rps. acidophila* and *Rb. sphaeroides*. The tilt angles resulting from these simulations can be seen in Fig. 2 B. The *Rps. acidophila*, *Rb. sphaeroides*, and *Phsp. molischianum* systems equilibrated to final tilt angles of $8.6^\circ \pm 0.4^\circ$, $12.9^\circ \pm 0.5^\circ$, and $11.2^\circ \pm 0.3^\circ$, respectively. These results further suggest that all LH2s can induce curvature, but that the extent of curvature varies among species.

Protein-lipid interactions

An analysis of hydrogen-bond formation between protein and lipids was also carried out. As many as 200 hydrogen bonds total formed between all seven LH2s and lipids over the course of each simulation; these bonds were equally distributed between POPE and POPG lipid molecules, indicating no preferential binding for either lipid type to LH2 (see Fig. S1 in the Supporting Material). Although the number of hydrogen bonds was similar for all three species, they are distributed differently in each, as seen in Fig. S2. For *Rps. acidophila* LH2, an equal number of bonds between lipid and the cytoplasmic half and the periplasmic half of the protein form; however, in *Phsp. molischianum* and *Rb. sphaeroides* LH2, approximately twice the number of bonds are formed on the cytoplasmic half compared to the periplasmic half. The greater binding of lipids on the cytoplasmic half of LH2 for the latter two species likely results from a greater number of charged residues compared to *Rps. acidophila* LH2, and may enhance the curvature by amplifying the wedge shape of *Phsp. molischianum* and *Rb. sphaeroides* LH2.

Simulations of *Rps. acidophila* and *Phsp. molischianum* charged-residue mutants

Modified versions of the *Rps. acidophila* LH2 were constructed and simulated. These modified LH2s fall into two categories: LH2s in which charged residues were mutated into alanine, and LH2s in which charged residues were changed to uncharged analogs. These simulations were identical to the closely packed LH2 simulations, except that the wild-type LH2s were replaced with these modified versions.

The alanine-replacement mutants were found to nearly eliminate curvature for *Rps. acidophila*; over 13 ns, the LH2s stabilized to a final tilt angle of $\sim 3.0^\circ$, giving a radius of curvature of 1446 Å, quite shallow compared to the wild-type system. One of these mutant LH2s contained no charged residues, i.e., all of the charged residues (glutamate, aspartate, lysine, arginine) were mutated to alanine. The original and altered amino-acid sequences are shown in

Fig. 1. This mutation did not appear to destabilize the LH2s (see Fig. S3 for root mean-square deviation data), but perturbed the interactions of neighboring LH2s such that it reduced their tilting behavior. The second mutant contained no charged residues on the cytoplasmic side, but the periplasmic charged residues (which are accessible to solvent and not well conserved) were left intact. The behavior of the two mutants was nearly identical, the first giving a final tilt angle of $3.4^\circ \pm 0.4^\circ$ and the second giving $2.9^\circ \pm 0.3^\circ$. A mutant version of *Phsp. molischianum* was also constructed in which all of its cytoplasmic charged residues were mutated to alanine. This mutation reduced, but did not eliminate, the curvature-inducing behavior of *Phsp. molischianum* LH2, decreasing the final tilt angle from $11.2^\circ \pm 0.3^\circ$ to $8.6^\circ \pm 0.4^\circ$. The *Rps. acidophila* neutral LH2 simulation showed reduced curvature, with a final tilt angle of $6.0^\circ \pm 0.3^\circ$, but the effect was less dramatic than for the alanine-replacement simulation; the *Phsp. molischianum* neutral LH2s showed roughly the same curvature ($10.7^\circ \pm 0.3^\circ$) as the wild-type *Phsp. molischianum* LH2s. The charged-residue mutant results are shown in Fig. 2, C and D. These mutations also resulted in the formation of fewer hydrogen bonds between LH2 and lipids (as much as 33% less in the case of the *Rps. acidophila* alanine-replacement mutant, see Fig. S4). This reduction was greater for the cytoplasmic half of the protein than the periplasmic half, thereby also reducing any potential contribution to LH2's effective shape. The fact that removal of the charged residues changed the overall curvature suggests that electrostatics plays a role in curvature formation. That the mutant systems behaved differently from the neutral systems implies that shape is also important, as the neutral LH2s preserved the shape of

the LH2 protein whereas the mutant versions replaced bulky side chains by smaller alanine residues.

Analysis of nonbonded forces in the simulations points to electrostatics as the driving force responsible for LH2 curvature. In each system, we observe that the radial component of the total electrostatic force acting on the top, cytoplasmic half of an outer ring LH2 is always directed outward, whereas the force acting on the bottom, periplasmic half is directed inward; this is just the pattern of forces needed to produce the observed LH2 tilting. When van der Waals forces are added in, the total force experienced by an LH2 is quite small, which is reasonable, given the subtle nature of the LH2 rearrangement seen in the simulations. Although the variance of the time series is appreciable, the averages show again that the total forces acting on the top and bottom halves of an LH2 would produce tilting in the expected direction. This data is provided in Fig. S5 and Fig. S6.

It seems likely that LH2-LH2 packing is also in some way responsible for curvature. In the cases of *Phsp. molischianum* and *Rb. sphaeroides*, the LH2s are already slightly wedge-shaped, with small protrusions on the cytoplasmic side that prohibit the proteins from packing as closely on top as they do on the bottom (an illustration of the radial profiles of each LH2 is given in Fig. S7). *Rps. acidophila* LH2 is slightly wedge-shaped, but in the opposite orientation, so its curvature cannot be explained by shape alone. However, all three proteins have many conserved charged residues on the cytoplasmic side, and the interaction of these residues may also modify packing in this region. We observe interactions between these residues in, for example, the formation of some inter-LH2 salt bridges (primarily β ASP17- β ARG20 in *Rps. acidophila* and β ASP18- α LYS4

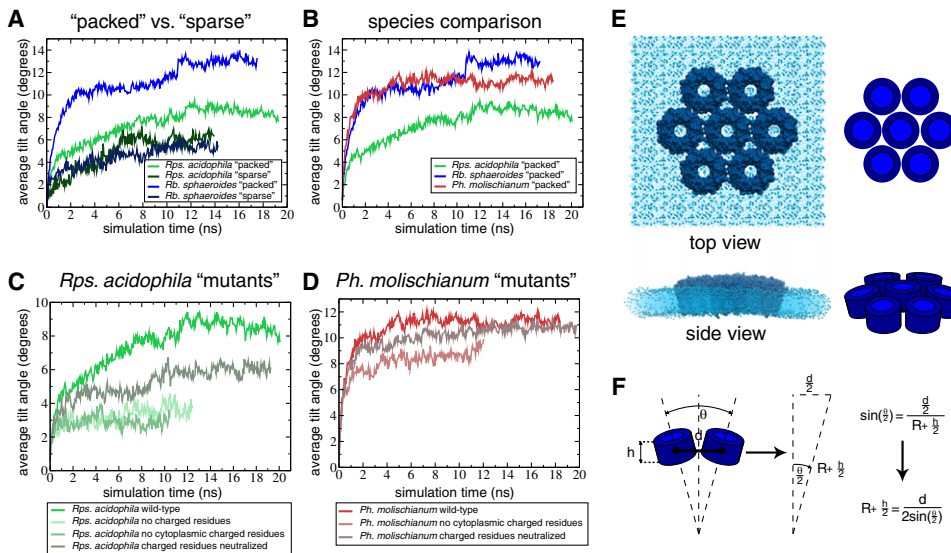


FIGURE 2 (A) Tilt angle versus simulation time for *Rps. acidophila* and *Rb. sphaeroides* sparse and packed configurations. In the sparse configuration, *Rps. acidophila* and *Rb. sphaeroides* equilibrated to final angles of $6.0^\circ \pm 0.4^\circ$ and $5.4^\circ \pm 0.3^\circ$, respectively; in the packed configuration, *Rps. acidophila* equilibrated to $8.6^\circ \pm 0.4^\circ$ and *Rb. sphaeroides* equilibrated to $12.9^\circ \pm 0.5^\circ$. (B) Tilt angle versus time for the packed configuration for *Rps. acidophila*, *Rb. sphaeroides*, and *Phsp. molischianum*. These systems equilibrated to final tilt angles of $8.6^\circ \pm 0.4^\circ$, $12.9^\circ \pm 0.5^\circ$, and $11.2^\circ \pm 0.3^\circ$, respectively. (C and D) Tilt angle versus time for *Rps. acidophila* and *Phsp. molischianum* charged-residue mutants. Mutating the (largely conserved) charged residues on the cytoplasmic side of LH2 to alanine substantially reduced the curvature-inducing properties of both LH2 species. Neutralizing

the charged residues reduced curvature for *Rps. acidophila* but not for *Phsp. molischianum*, suggesting that electrostatic forces from charged residues play a greater role in *Rps. acidophila* than in *Phsp. molischianum*. (E) Simulation system for *Phsp. molischianum* showing the top view of the starting configuration and the side view showing curvature at the end of the simulation, with cartoon showing the tilting of the LH2s. (F) Cartoon and derivation of Eq. 1.

and β ASP18- β LYS21 in *Phsp. molischianum*) and of stacking interactions between neighboring β ARG20s in *Rps. acidophila*. That the LH2 charge modifications affect packing is suggested by the van der Waals interaction energy of the seven LH2s, which is minimized as the LH2s seek their optimal packing. The van der Waals energy of the top half of the LH2s is consistently higher for the wild-type *Rps. acidophila* and *Phsp. molischianum* cases and lower for the chargeless mutant and neutral versions, suggesting better cytoplasmic packing for the modified LH2s (see Fig. S8). By contrast, the van der Waals energies for the bottom halves of the modified LH2s are more similar to the respective wild-types.

Simulation of an *Rps. acidophila* LH1 monomer surrounded by LH2s

Although multiple LH2s and a single RC-LH1-PufX dimer have been shown to induce membrane curvature in simulation (7), chromatophores typically contain mixtures of both proteins. The oligomeric state of LH1 varies depending on species, with monomeric LH1 typically found in species with lamellar chromatophores, e.g., *Rps. acidophila*, *Phsp. molischianum*, and *Rhodospseudomonas palustris*, whereas dimeric LH1 is found in species with spherical chromatophores, e.g., *Rb. sphaeroides* and *Rhodobacter blasticus* (25–28). In AFM images of different species, distinct organizations of monomeric or dimeric LH1 and LH2s become apparent (25,27,29). For example, in *Rb. sphaeroides* stacks of LH1 dimers are seen, with large fields of LH2s in between the stacks (27). In addition, in *Phsp. molischianum*, *Rhodospirillum photometricum*, and *Rps. palustris*, regions of well-mixed LH1 monomers and LH2s are observed, along with some regions of crystallized LH2s or LH1s alone, depending on their relative concentration (25,26,28,29). In the mixed regions, each LH1 contacts zero or one other LH1 and between six and seven LH2s (25,29).

To characterize an LH1 monomer's potential for curvature formation, we simulated a system of a single LH1 monomer surrounded by seven LH2s, all from *Rps. acidophila*, based on the organization observed in AFM images (25,29). As there is currently no structure for LH1 from *Rps. acidophila*, a homology model based on a previously constructed *Rb. sphaeroides* LH1 was built (see Methods) (7). The LH2s were placed around LH1 in a closely packed configuration, with no lipid between each LH2 and LH1. After initial equilibration, the system was simulated for 14 ns. We observed no net curvature of the proteins or membrane in the simulation; the final state of the system is shown in Fig. 3. We also measured the average tilt angle of the LH2s with respect to LH1 over time (see Fig. 3). After a period where the angle fluctuates around zero, the profile becomes nearly flat, with the angle stabilizing at $\sim 2.5^\circ$. This angle corresponds to a chromatophore radius of $>2000 \text{ \AA}$, larger even than that observed for the chargeless LH2 mutants. By examining their

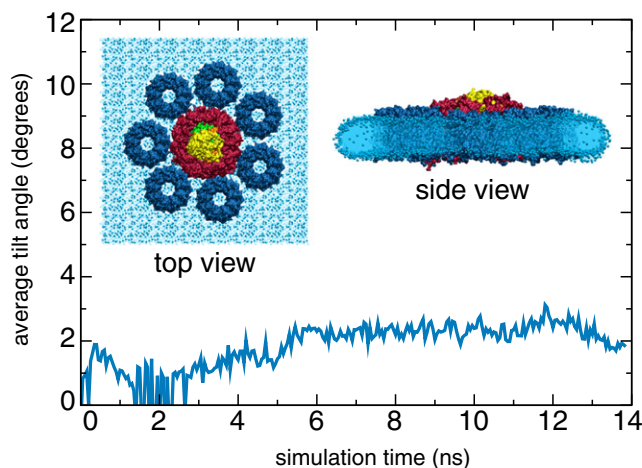


FIGURE 3 Simulation of an LH1 monomer surrounded by LH2s. The graph plots the average tilt angle of LH2 with respect to LH1 over time. The inset shows the starting arrangement of the system as viewed from the top and the system after 14 ns viewed from the side. LH2s are colored in blue, LH1 is colored in red, and the RC in yellow, green, and orange. The LH2s and the membrane remain flat.

sequences, we find that LH1 β contains 13 more residues than LH2 β ; our model places most of the additional residues above the membrane on the cytoplasmic side. Therefore, although LH1 β contains some charged residues on the cytoplasmic side, they are spatially separated from the LH2 β charged residues. This separation explains why the presence of these charged residues should not affect LH1-LH2 packing on the cytoplasmic side.

DISCUSSION

In this report, we have summarized the results of several MD simulations that probed the formation of curvature by LH2s and by LH1 monomers with LH2s. We found that aggregates of seven hexagonally packed LH2s were capable of inducing curvature in all species examined (*Rb. sphaeroides*, *Phsp. molischianum*, and *Rps. acidophila*). We also found that the extent of this curvature is strengthened by close-packing and is likely caused by a combination of the physical shape of the proteins and interactions involving conserved charged residues on the cytoplasmic side of LH2. By contrast, an LH1 monomer surrounded by seven LH2s was not found to induce curvature, likely due to the absence of the electrostatic interactions seen in the LH2-only system.

We have suggested that chromatophore shape may depend on the organization of the photosynthetic proteins. This suggestion is based on observation of AFM images of chromatophore membranes, which have shown LH1 dimers in species with vesicular chromatophores (the LH1-only species *Rhodospirillum rubrum* excepted) and LH1 monomers in species with lamellar chromatophores (25,27,28). It has been seen both in simulation and experiment that LH1 dimers are bent along their dimerizing interface and

induce curvature on their own (7,30,31), forming tubular chromatophores in LH2⁻ *Rb. sphaeroides* mutants (5,6,32). Our results indicate, however, that LH1 monomers do not induce curvature, at least not when interacting with LH2s. We suggest that the inability of LH1 monomers to curve limits the curvature of LH2s in species with flat chromatophores; in contrast, the ability of LH1 dimers to curve may reinforce the curvature of LH2s in species with vesicular chromatophores. In support of this suggestion, Monte Carlo simulations of chromatophore proteins have also shown a connection between the local curvature generated by LH1 with LH2 and global curvature (8). It must also be noted that other factors may determine chromatophore shape, such as lipid distribution and ion concentration, which are not accessible to simulations of the scale described here. Additionally, our 20-ns simulations are too brief to permit diffusion of lipids or proteins, and so cannot address how longer-term rearrangement of these factors affects the evolution of curvature in the forming chromatophore. Nevertheless, our results support the idea that the presence of closely packed LH2 and the oligomeric state of LH1 play roles in determining chromatophore shape.

There are still many unanswered questions regarding chromatophore shape and formation, and several experimental observations that cannot be explained by the simple ideas suggested in this article. The chromatophores of species like *Rps. acidophila*, *Phsp. molischianum*, and *Rps. palustris* are not merely flat, but form complex stacked lamellar folds, not unlike the grana seen in chloroplasts. It has been suggested that the stacking of these lamellae depend on some adhesion effect between LH1 monomers, analogous to the adhesion effect of the light-harvesting complexes in chloroplasts (33,34), and it has been shown in both systems that this adhesion is very sensitive to ion concentration. It is plausible that the presence of LH1 monomers is necessary for the formation of lamellar chromatophores, and that adhesion of the lamellae would overwhelm any curvature caused by LH1 or LH2. The LH1-only species *Rs. rubrum* and *Rps. viridis* both have monomeric LH1s (and no LH2s), but *Rs. rubrum* forms vesicular chromatophores whereas *Rps. viridis* forms lamellar folds (35–37); it seems therefore that the presence of LH1 monomers does not guarantee lamellae, and that chromatophore formation in these species must depend on other, more subtle factors than protein organization alone. The wealth of experimental observations on *Rb. sphaeroides* mutants provides its own set of mysteries. That wild-type bacteria and LH2-only mutants form small vesicles, whereas LH1-dimer-only mutants form tubules (5,6), is sensible according to our model. However, that LH1-monomer-only mutants (in which the dimerizing agent PufX is deleted) form large micrometer-sized vesicles or flat sheets (32), and that mutants lacking PufX but retaining LH2s have been observed to form vesicles of unreported size (38), are observations that are more difficult to explain. There remains much work to be done, both experimentally and computationally,

to gain further insight into the function and ontology of these complex supramolecular assemblies. We intend to move to simulations of larger aggregates of LH2s and LH1 monomers and dimers in different arrangements. Some questions may also be addressable using coarse-grained representations of the proteins, in the spirit of the simulations reported in the literature (39,40), and such work is currently underway. Our results so far are unable to explain the vast and variegated cases of chromatophore formation observed in the literature, but we would like to continue studying the issue of chromatophore shape and hope that experimentalists may be inspired to continue to examine chromatophore formation via mutation studies.

SUPPORTING MATERIAL

Eight figures are available at [http://www.biophysj.org/biophysj/supplemental/S0006-3495\(09\)01451-9](http://www.biophysj.org/biophysj/supplemental/S0006-3495(09)01451-9).

We thank Jen Hsin, Christopher Harrison, and Melih Sener for many useful discussions. Molecular images in this article were generated with the molecular graphics program VMD (41).

This work is supported by the National Institutes of Health (grant No. P41-RR05969) and the National Science Foundation (grant No. MCB-0744057). This research used resources from the Argonne Leadership Computing Facility at Argonne National Laboratory, which is supported by the Office of Science of the U.S. Department of Energy under contract No. DE-AC02-06CH11357. The authors also acknowledge supercomputer time provided by Pittsburgh Supercomputing Center and the National Center for Supercomputing Applications via Large Resources Allocation Committee grant No. MCA93S028 and the Turing Xserve Cluster, owned by the University of Illinois.

REFERENCES

- Hu, X., T. Ritz, A. Damjanović, F. Autenrieth, and K. Schulten. 2002. Photosynthetic apparatus of purple bacteria. *Q. Rev. Biophys.* 35:1–62.
- Cogdell, R. J., A. Gall, and J. Köhler. 2006. The architecture and function of the light-harvesting apparatus of purple bacteria: from single molecules to in vivo membranes. *Q. Rev. Biophys.* 39:227–324.
- Fromme, P., and I. Grotjohann. 2008. Overview of photosynthesis. In *Photosynthetic Protein Complexes*. P. Fromme, editor. Wiley-VCH Verlag, Weinheim, Germany.
- Oelze, J., and G. Drews. 1972. Membranes of photosynthetic bacteria. *Biochim. Biophys. Acta.* 265:209–239.
- Kiley, P. J., A. Varga, and S. Kaplan. 1988. Physiological and structural analysis of light-harvesting mutants of *Rhodobacter sphaeroides*. *J. Bacteriol.* 170:1103–1115.
- Hunter, C. N., J. D. Pennoyer, J. N. Sturgis, D. Farrelly, and R. A. Niederman. 1988. Oligomerization states and associations of light-harvesting pigment protein complexes of *Rhodobacter sphaeroides* as analyzed by lithium dodecyl sulfate-polyacrylamide gel electrophoresis. *Biochemistry.* 27:3459–3467.
- Chandler, D., J. Hsin, C. B. Harrison, J. Gumbart, and K. Schulten. 2008. Intrinsic curvature properties of photosynthetic proteins in chromatophores. *Biophys. J.* 95:2822–2836.
- Frese, R. N., J. C. Pàmies, J. D. Olsen, S. Bahatyrova, C. D. van der Weij-de Wit, et al. 2008. Protein shape and crowding drive domain formation and curvature in biological membranes. *Biophys. J.* 94:640–647.

9. Al-Bayatti, K. K., and J. Y. Takemoto. 1981. Phospholipid topography of the photosynthetic membrane of *Rhodospseudomonas sphaeroides*. *Biochemistry*. 20:5489–5495.
10. Onishi, J. C., and R. A. Niederman. 1981. *Rhodospseudomonas sphaeroides* membranes: alterations in phospholipid composition in aerobically and phototrophically grown cells. *J. Bacteriol.* 149:831–839.
11. Russell, N. J., J. K. Coleman, T. D. Howard, E. Johnston, and R. J. Cogdell. 2002. *Rhodospseudomonas acidophila* strain 10050 contains photosynthetic LH2 antenna complexes that are not enriched with phosphatidylglycerol, and the phospholipids have a fatty acyl composition that is unusual for purple non-sulfur bacteria. *Biochim. Biophys. Acta.* 1556:247–253.
12. Kwa, L. G., D. Wegmann, B. Brugger, F. T. Wieland, G. Warner, et al. 2008. Mutation of a single residue, β -glutamate-20, alters protein-lipid interactions of light harvesting complex II. *Mol. Microbiol.* 67:63–77.
13. Marinetti, G. V., and K. Cattieu. 1981. Lipid analysis of cells and chromatophores of *Rhodospseudomonas sphaeroides*. *Chem. Phys. Lipids.* 28:241–251.
14. Li, L., I. Vorobyov, A. D. M. Jr., and T. W. Allen. 2008. Is arginine charged in a membrane? *Biophys. J.* 92:11–13.
15. Phillips, J. C., R. Braun, W. Wang, J. Gumbart, E. Tajkhorshid, et al. 2005. Scalable molecular dynamics with NAMD. *J. Comput. Chem.* 26:1781–1802.
16. MacKerell, Jr., A. D., D. Bashford, M. Bellott, R. L. Dunbrack, Jr., J. Evanseck, et al. 1998. All-atom empirical potential for molecular modeling and dynamics studies of proteins. *J. Phys. Chem. B.* 102:3586–3616.
17. MacKerell, Jr., A. D., M. Feig, and C. L. Brooks, III. 2004. Extending the treatment of backbone energetics in protein force fields: limitations of gas-phase quantum mechanics in reproducing protein conformational distributions in molecular dynamics simulations. *J. Comput. Chem.* 25:1400–1415.
18. Darden, T., D. York, and L. Pedersen. 1993. Particle mesh Ewald. An $N \cdot \log(N)$ method for Ewald sums in large systems. *J. Chem. Phys.* 98:10089–10092.
19. Hu, X., and K. Schulten. 1998. A model for the light-harvesting complex I (B875) of *Rhodobacter sphaeroides*. *Biophys. J.* 75:683–694.
20. Jamieson, S. J., P. Wang, P. Qian, J. Y. Kirkland, M. J. Conroy, et al. 2002. Projection structure of the photosynthetic reaction center-antenna complex of *Rhodospirillum rubrum* at 8.5 Å resolution. *J. Mol. Biol.* 21:3927–3935.
21. Roszak, A. W., T. Howard, J. Southall, A. T. Gardiner, C. J. Law, et al. 2003. Crystal structure of the RC-LH1 core complex from *Rhodospseudomonas palustris*. *Science.* 302:1969–1972.
22. Scheuring, S., J. Seguin, S. Marco, D. Lévy, B. Robert, et al. 2003. Nanodissection and high-resolution imaging of the *Rhodospseudomonas viridis* photosynthetic core-complex in native membranes by AFM. *Proc. Natl. Acad. Sci. USA.* 100:1690–1693.
23. Bahatyrova, S., R. N. Frese, K. O. van der Werf, C. Otto, C. N. Hunter, et al. 2004. Flexibility and size heterogeneity of the LH1 light harvesting complex revealed by atomic force microscopy. *J. Biol. Chem.* 279:21327–21333.
24. Scheuring, S., and J. Sturgis. 2005. Chromatic adaptation of photosynthetic membranes. *Science.* 309:484–487.
25. Gonçalves, R. P., A. Bernadac, J. N. Sturgis, and S. Scheuring. 2005. Architecture of the native photosynthetic apparatus of *Phaeospirillum molischianum*. *J. Struct. Biol.* 152:221–228.
26. Scheuring, S., R. P. Gonçalves, V. Prima, and J. N. Sturgis. 2006. The photosynthetic apparatus of *Rhodospseudomonas palustris*: structures and organization. *J. Mol. Biol.* 358:83–96.
27. Bahatyrova, S., R. N. Frese, C. A. Siebert, J. D. Olsen, K. O. van der Werf, et al. 2004. The native architecture of a photosynthetic membrane. *Nature.* 430:1058–1062.
28. Scheuring, S., D. Lévy, and J.-L. Rigaud. 2005. Watching the components of photosynthetic bacterial membranes and their in situ organization by atomic force microscopy. *Biochim. Biophys. Acta.* 1712:109–127.
29. Scheuring, S., J. Rigaud, and J. Sturgis. 2004. Variable LH2 stoichiometry and core clustering in native membranes of *Rhodospirillum photometricum*. *EMBO J.* 23:4127–4133.
30. Qian, P., P. A. Bullough, and C. N. Hunter. 2008. Three-dimensional reconstruction of a membrane-bending complex: the RC-LH1-PufX core dimer of *Rhodobacter sphaeroides*. *J. Biol. Chem.* 283:14002–14011.
31. Hsin, J., J. Gumbart, L. G. Trabuco, E. Villa, P. Qian, et al. 2009. Protein-induced membrane curvature investigated through molecular dynamics flexible fitting. *Biophys. J.* 97:321–329.
32. Siebert, C. A., P. Qian, D. Fotiadis, A. Engel, C. N. Hunter, et al. 2004. Molecular architecture of photosynthetic membranes in *Rhodobacter sphaeroides*: the role of PufX. *EMBO J.* 23:690–700.
33. Varga, A. R., and L. A. Staehelin. 1985. Membrane adhesion in photosynthetic bacterial membranes. Light harvesting complex I (LH1) appears to be the main adhesion factor. *Arch. Microbiol.* 141:290–296.
34. Mullet, J. E. 1983. The amino acid sequence of the polypeptide segment which regulates membrane adhesion (grana stacking) in chloroplasts. *J. Biol. Chem.* 258:9941–9948.
35. Holt, S. C., and A. G. Marr. 1965. Effect of light intensity on the formation of intracytoplasmic membrane in *Rhodospirillum rubrum*. *J. Bacteriol.* 89:1421–1429.
36. Konorty, M., N. Kahana, A. Linaroudis, A. Minsky, and O. Medalia. 2008. Structural analysis of photosynthetic membranes by cryo-electron tomography of intact *Rhodospseudomonas viridis* cells. *J. Struct. Biol.* 161:393–400.
37. Fotiadis, D., P. Qian, A. Philippsen, P. A. Bullough, A. Engel, et al. 2004. Structural analysis of the reaction center light-harvesting complex I photosynthetic core complex of *Rhodospirillum rubrum* using atomic force microscopy. *J. Biol. Chem.* 279:2063–2068.
38. Barz, W., F. Francia, G. Venturoli, B. A. Melandri, A. Vermeglio, et al. 1995. Role of PufX protein in photosynthetic growth of *Rhodobacter sphaeroides*. I. PufX is required for efficient light-driven electron transfer and photophosphorylation under anaerobic conditions. *Biochemistry.* 34:15235–15247.
39. Arkhipov, A., Y. Yin, and K. Schulten. 2008. Four-scale description of membrane sculpting by BAR domains. *Biophys. J.* 95:2806–2821.
40. Reynwar, B. J., G. Illya, V. A. Harmandaris, M. M. Müller, K. Kremer, et al. 2007. Aggregation and vesiculation of membrane proteins by curvature-mediated interactions. *Nature.* 447:461–464.
41. Humphrey, W., A. Dalke, and K. Schulten. 1996. VMD—visual molecular dynamics. *J. Mol. Graph.* 14:33–38.